

## SYNTHESIS AND CHARACTERIZATION OF RARE EARTH SUBSTITUTED M -TYPE (Sr-Ba) HEXAFERRITES

H. M. KHAN<sup>a</sup>, Z. MIRRANI<sup>b</sup>, A. WAHEED<sup>c</sup>, J. AHMAD<sup>d</sup>, M. E. MAZHAR<sup>d,\*</sup>, M. N. USMANI<sup>d</sup>, I. SYED<sup>e</sup>, S. BAKHTAWAR<sup>d</sup>, I. AHMAD<sup>d</sup>, W. ABBAS<sup>d</sup>, R. NAZ<sup>f</sup>, S. AHMAD<sup>g</sup>, M. MAHMOOD<sup>d</sup>,

<sup>a</sup>Department of Physics, The Islamia University of Bahawalpur, Bahawalpur-63100, Pakistan

<sup>b</sup>Department of Physics, Allama Iqbal Open University, Islamabad, Pakistan

<sup>c</sup>Department of Geotechnical Engineering, MCE (NUST), Risalpur, Pakistan

<sup>d</sup>Department of Physics, Bahauddin Zakariya University, Multan, Pakistan

<sup>e</sup>Department of Computer Science, The Superior College Lahore, Pakistan

<sup>f</sup>School of Material Science and Engineering, Shanghai Jiao Tong University, Dongchuan Road, Shanghai, 200240, P. R. China

<sup>g</sup>Department of Building and Architectural Engineering, UCE&T, Bahauddin Zakariya University, Multan, Pakistan

Effect of Rare earth elements (PrMn) substitution on the structural of Electrical and Dielectric properties  $\text{Sr}_{0.5-x}\text{Ba}_{0.5}\text{Pr}_x\text{Mn}_y\text{Fe}_{12-y}\text{O}_{19}$  ( $x = 0.00-0.10$ ;  $y = 0.00-1.00$ ) Hexa-ferrites prepared by sol-gel auto combustion is reported. The synthesized samples were characterized by Fourier Transform Infrared (FTIR) Spectroscopy, X-ray diffraction (XRD), scanning electron microscopy (SEM), AC and DC analysis. The XRD analysis confirmed the formation of single and double phase M-type Hexa-ferrite structures. The lattice parameters were found to be increasing as Rare earth (PrMn) contents were increasing, which is attributed to the ionic sizes of the implicated cations. The rare earth (PrMn) seems to be entirely soluble in the lattice. SEM revealed that the grain size decreased with increasing rare earth (PrMn) substitution. The coercivity values ( $780-1077\text{cm}^{-1}$ ) of all sample lies in the range of M-type hexa-ferrite's, which indicated that an increase of anisotropy was achieved by substitution of rare earth doping, while the size of particles drastically reduced from 10 to 1  $\mu\text{m}$ . The increased anisotropy and fine particle size is useful for many applications such as improving signal noise ratio of recording devices.

(Received July 11, 2020; Accepted October 3, 2020)

**Keywords:** M-type hexaferrite, Sol-gel, XRD, FTIR, SEM, Electrical and Dielectric Properties

### 1. Introduction

Ferrites are attractive types of magnetic materials amongst researchers due to their functionality in advanced electrical devices. A subclass of ferrites i.e. hexaferrites contain most unique electrical and magnetic properties and they are considered to be very attractive type of magnetic materials having masses of applications in different electric devices including but not limited to cores of transformer, noise filters/ isolators, magnetic memory devices, magnetic recording media, and permanent magnets magneto-optical devices etc. There are several studies on the magnetic properties of hexagonal ferrites have been reported so far, showing improved magnetic, structural and microwave absorption properties with modification in structure by doping of rare earth metals [1-4]. Furthermore, simple and cheap manufacturing techniques can yield low cost and high power at low dielectric loss functionalities from these hexaferrite materials. Studies on  $\text{BaFe}_{12}\text{O}_{19}$  showed that nano sized hexagonal  $\text{BaFe}_{12}\text{O}_{19}$  has a single magnetic domain and high anisotropy due to which it offers outstanding magnetic properties which absolutely depend upon

\* Corresponding author: dr.ehsan@bzu.edu.pk

the mean grain size and morphology of the synthesized materials [5–9]. The electrical properties can be altered by substituting fractional amounts of rare earth elements [10]. In this study, the sol-gel method has been used to synthesize strontium barium hexaferrites. M-type hexaferrites with Sr, Ba base have not been reported so far except Iqbal et al<sup>[11]</sup>. Strontium and barium are selected as base due to their fundamental properties, and the combination of divalent and rare earth improves electrical and magnetic properties [12, 13]. The high electrical resistivity and low dielectric losses are obtained in this study, which are helpful in many applications of microwave absorption, recording media, optical wave guides and permanent magnets [14]. The aim of the present study is to synthesize and to investigate the effect of rare earth substituted M-type (Sr-Ba) Hexaferrites effect of PrMn substitution on electrical and dielectric properties as well as room temperature-dependent magnetization of Sr-based M-type hexaferrites. It was reported that substitution of Praseodymium results in inhibiting the grain growth where by increasing Praseodymium concentration, the average grain size decreases.

## 2. Experiment details

### 2.1. Sample preparation

M-type hexaferrites with chemical compositions of  $\text{Sr}_{0.5-x}\text{Ba}_{0.5}\text{Pr}_x\text{Mn}_y\text{Fe}_{12-y}\text{O}_{19}$  ( $x=0.00-0.10$  and  $y=0.0-1.00$ ) were synthesized by the sol-gel auto-combustion technique [15]. The reagents used for the synthesis include Iron Nitrate  $\text{Fe}(\text{NO}_3)_3$  Manganese Chloride Tetra hydrate ( $\text{MnCl}_4$ ), Barium Nitrate ( $\text{Ba}(\text{NO}_3)_2$ ), Citric Acid  $\text{C}_6\text{H}_8\text{O}_7$ , Praseodymium Nitrate Hex hydrate  $\text{Pr}(\text{NO}_3)_2 \cdot \text{H}_2\text{O}$ , Ammonium oxalate monohydrate  $(\text{NH}_4)_2\text{C}_2\text{O}_4 \cdot \text{H}_2\text{O}$  and  $\text{Sr}(\text{NO}_3)_2 \cdot 9\text{H}_2\text{O}$ . The stoichiometric amounts of starting materials were dissolved in 100 ml deionized water. The stock solutions of other salts were prepared accordingly. As  $\text{Pr}_2\text{O}_3$  is insoluble in water, therefore it was first dissolved in nitric acid at  $80^\circ\text{C}$  and poured into the prepared solution. To maintain the pH value at 7, an aqueous ammonia solution (at a ratio of 4:6) was added drop wise while stirring at  $80^\circ\text{C}$  constantly. After stirring about 6-8 hours the sol was formed which was allowed to gel at  $80^\circ\text{C}$ . The gel was then burnt to get desired ceramic powder at  $300^\circ\text{C}$  for three hours in furnace. The obtained material was in powder form which was further ground in an agate mortar and pestle for 30 min. And finally, the homogenized powder was then sintered at  $950^\circ\text{C}$  at 8h. The Pellets of 8mm diameter of the materials were prepared by using the hydraulic press at 80KN pressure at room temperature. Polyvinyl alcohol was used as (3–5 wt%) for the preparation of the pellets. The binder evaporated at  $250^\circ\text{C}$  as the pellets were re-sintered at  $950^\circ\text{C}$  for 8h.

### 2.1. Characterization

X-ray diffraction was performed by Shimadzu X-ray diffractometer prepared using  $\text{CuK}_\alpha$  radiation  $\lambda = 1.5406 \text{ \AA}$ . With the help of Scherrer's formula (eq. 1) we calculated the crystallite size. [16].

$$D = \frac{k\lambda}{\beta \cos\theta} \quad (1)$$

where, 'K' indicates the shape constant,  $\lambda$  shows the wavelength,  $\beta$  is represents FWHM of reflection peak and the Bragg angle is denoted by  $\theta$ .

Reflectivity responses of all prepared materials were measured on FTIR spectrometer (Bruker, Vertex- 80V) in frequency range of  $10-15,500 \text{ cm}^{-1}$  and KBr beam splitter was used. In the far-infrared range i. e. ( $5-400 \text{ cm}^{-1}$ ), A DLATGS detector with Multilayer and Mylar beam splitter were employed. All the measurements were carried out at room temperature under vacuum.

Furthermore, the DC resistivity was calculated using two-point probe technique using Keithley Source Meter model 2400. The dielectric response was also measured using LCR meter model no 8101 Gw INSTRON. The dielectric loss and capacitance 'C' were calculated in the frequency range of 1Hz to 1GHz. Using the following formula to calculated dielectric constant ' $\epsilon_r$ '.

$$\epsilon_r = \frac{Cd}{A\epsilon_0} \quad (2)$$

where  $d$  is the thickness of the sample,  $C$  is capacitance and  $A$  indicates the area of cross section of the sample pellet and  $\epsilon_0$  would explain the dielectric permittivity of the free space. AC conductivity was measured using following relation [18].

$$\sigma_{ac} = 2\pi f \tan \delta \quad (3)$$

### 3. Results and discussions

#### 3.1 X-Ray Diffraction

The XRD patterns of pure chemical and rare earth elements composition of  $(\text{Sr}_{0.5-x}\text{Pr}_x\text{Ba}_{0.5}\text{Fe}_{12-y}\text{Mn}_y\text{O}_{19})$  is are shown in Fig. 1, where  $(X=0.00-0.1, Y=0.0-1.0)$  and the corresponding values of lattice parameters, relative intensities and crystal system have been shown in table.1. The analysis of these measurements reveal that all the peaks match well with the standard M-type barium hexa-ferrites JCPDS card No.PDF (00-001-0574) [21, 23]. It is observed that the samples  $(\text{Sr}_{0.5-x}\text{Pr}_x\text{Ba}_{0.5}\text{Fe}_{12-y}\text{Mn}_y\text{O}_{19})$ ,  $(x = 0.00-0.10; y = 0.00-1.00)$  have FCC single phase structure. As the dopant concentration is further increased i.e.  $(X=0.08 - 0.1)$ , a secondary phase appears. Secondary peaks were observed at  $2\theta = (30.06), (39.32), (34.7), (37.2)$  and  $(55.6)$  and their hkl value were calculated to be  $(111), (107), (200), (203)$  and  $(200)$ . Such reflection peaks are highlighted by putting ‘\*’ over them in the graph. These peaks were also indexed and matched to ICDD PDF#00-002-0692 of  $\text{PrFeO}_3$  material [24].

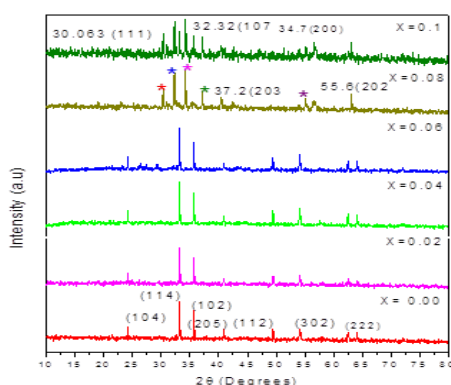


Fig. 1. XRD Patterns of  $\text{Sr}_{0.5-x}\text{Pr}_x\text{Ba}_{0.5}\text{Fe}_{12-y}\text{Mn}_y\text{O}_{19}$  where  $(x=0.00-0.1, y=0.0-1.0)$ .

##### 3.1.1. Lattice parameter

X-ray spectra were also used to calculate lattice parameters using Sherrer's equation. Fig. 2 shows the lattice constants of  $(\text{Sr}_{0.5-x}\text{Pr}_x\text{Ba}_{0.5}\text{Fe}_{12-y}\text{Mn}_y\text{O}_{19})$ ,  $(x = 0.00-0.10; y = 0.00-1.00)$  hexa-ferrites ranges from  $a = (5.93 - 5.94) \text{ \AA}$  and  $c = (23.28 - 23.32) \text{ \AA}$ , showing small variations from lattice constants of pure  $\text{BaFe}_{12}\text{O}_{19}$ . These small changes in the lattice constants appear by the variation between the ionic radii of  $\text{Pr}^{3+}$  ( $0.99 \text{ \AA}$ ) and  $\text{Fe}^{3+}$  ( $0.645 \text{ \AA}$ ). Such increase in lattice constants due to the substitution of rare earth element has also been observed by other researchers [25, 26]. It can be concluded from the absence of secondary phase from graph of hexaferrites having substitution in range of  $(x = 0.00-0.05; y = 0.00-0.06)$  that  $\text{Pr}^{3+}$  ions were successfully substituted the lattice ions of the hexa-ferrites [27].

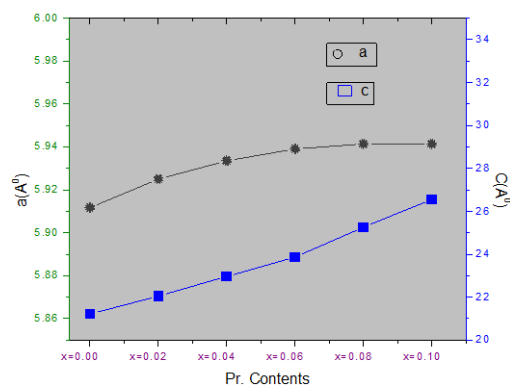


Fig. 2. Lattice parameters for  $(Sr_{0.5-x}Pr_xBa_{0.5}Fe_{12-y}Mn_yO_{19})$  where  $(x=0.00-0.1, y=0.0-1.0)$ .

### 3.2. Fourier Transform Infra-Red Spectroscopy of Ferrites

FTIR was used to obtain structural information about m-type phase formation. The effects of different additives on Hexagonal  $BaFe_{12}O_{19}$  (PrMn) structure, the infrared spectra contained by the frequency range  $4000\sim 400\text{cm}^{-1}$  of pure  $BaFe_{12}O_{19}$  and substituted rare earth (Pr, Mn) are shown in Fig. 3. The samples annealed  $950^\circ\text{C}$  exhibited  $\text{CO}_2$  vibration (peak at  $2372\text{cm}^{-1}$ ) and water absorption (peak above  $3500\text{cm}^{-1}$ ). Two most important combination bands indicate at  $660\text{cm}^{-1}$  and  $808\text{cm}^{-1}$  in the first four samples and while remaining two samples have absorption band at  $2159\text{cm}^{-1}$  and  $2372\text{cm}^{-1}$ . They were attributed to the asymmetric hydrogen method of  $BaFe_{12}O_{19}$  group (mix up because to Hexagonal structure). In FTIR spectra the absorption at  $2159$  and  $2372\text{cm}^{-1}$  were assigned to carbon dioxide ( $\text{CO}_2$ ). The bands at  $1750$  and  $1800\text{cm}^{-1}$  were assigned to the stretching vibrate of the carbon make double bond with oxygen ( $\text{C}=\text{O}$ ) bond of  $\text{CH}_3\text{COOH}$  with combination at  $1161\text{cm}^{-1}$  which was contributed by the single bond carbon and oxygen ( $\text{C}-\text{O}$ ) vibration of the acetic acid. The spreading vibration of the oxygen with single hydrogen ( $\text{O}-\text{H}$ ) bond appeared over range ( $3500-3800\text{cm}^{-1}$ ). The mix up bands approximately ( $1099-1996\text{cm}^{-1}$ ) and more at  $4000\text{cm}^{-1}$  can be described for the water absorption. However, no absorption bands observed at  $2159-2372\text{cm}^{-1}$ ,  $1099\text{cm}^{-1}$ , or above  $3500\text{cm}^{-1}$  in one of the samples. This obviously depicted that no sign left unreacted, as nitrates and acetates were useful as precursors in synthesized of  $BaFe_{12}O_{19}$  and its consequences [19, 20].

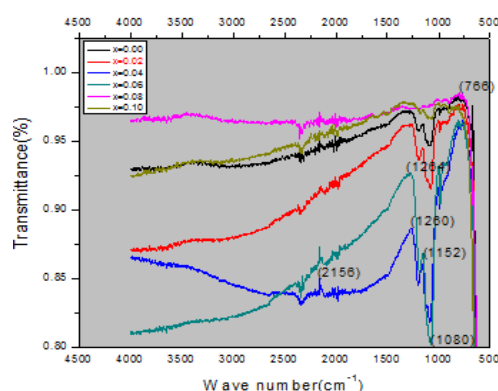


Fig. 3. FTIR Spectra of  $(Sr_{0.5-x}Pr_xBa_{0.5}Fe_{12-y}Mn_yO_{19})$  where  $x=0.00-0.1, y=0.0-1.0$ .

### 3.3. Scanning Electron Microscope (SEM)

SEM was used to study the surface morphology and shape of the particles formed by the sol-gel technique. SEM analysis of three selected samples and their compositions. (a)  $(Sr_{0.5}Ba_{0.5}Fe_{12}O_{19})$ , (b)  $(Sr_{0.46}Pr_{0.04}Ba_{0.5}Mn_{0.4}Fe_{11.6}O_{19})$  (c)  $(Sr_{0.40}Pr_{0.10}Ba_{0.5}Mn_{1.0}Fe_{11.0}O_{19})$  was performed. Fig. 4 (a,b,c) show the SEM images of the prepared materials at  $(Sr_{0.5-x}Pr_xBa_{0.5}Fe_{12-y}Mn_yO_{19})$ , ( $x=0.00-0.06; y=0.00-0.60$ ). Some particles show well defined hexagonal shapes whose size ranges

from 1-10  $\mu\text{m}$ . However, some small nanosized particles can also be observed. Pure hexaferrite has somewhat different morphology from the remaining two samples, where particles of regular size seem to merge together to make larger grains. While figures b and c show leaf like particles oriented in different directions. Also, many grains show hexagonal geometry. Such morphologies have also been reported for these materials in literature [28].

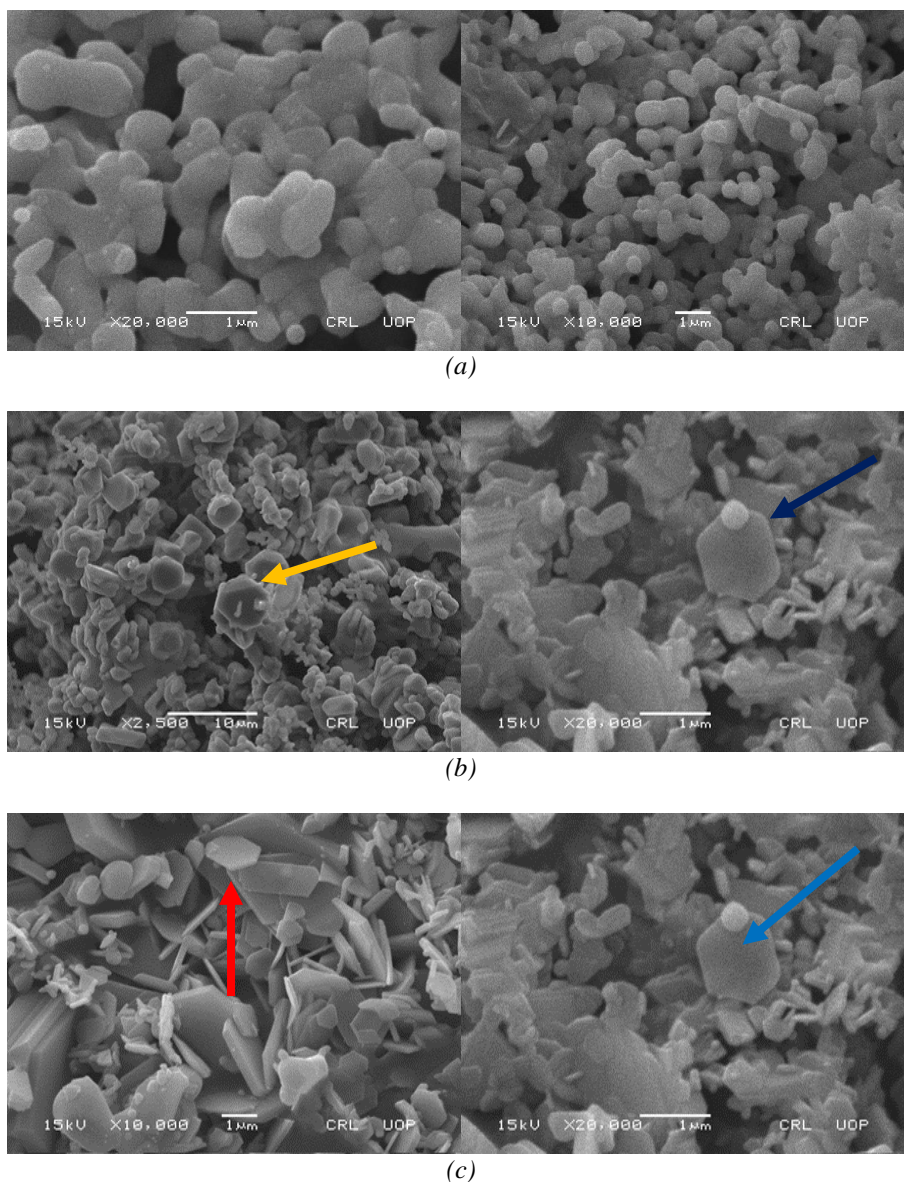


Fig. 4. (a, b, c) difference of room temperature resistivity ( $\text{Sr}_{0.5-x}\text{Pr}_x\text{Ba}_{0.5}\text{Fe}_{12-y}\text{Mn}_y\text{O}_{19}$ ) where  $X=0.00-0.1$ ,  $Y=0.0-1.0$ .

## 4. Electrical characterizations

### 4.1 Room Temperature Resistivity

Fig. 5 shows the variation indicates whether resistivity decrease or increases vs. Pr-concentration at 0 to 5 applied voltages correspondingly. On usual, it was observed that the room temperature resistivity enhanced with the increase of Pr-content from  $7 \times 10^{14}$ ,  $6 \times 10^{14}$ ,  $5 \times 10^{14}$  and from  $4 \times 10^{14} \Omega\text{-cm}$  to  $1 \times 10^{14} \Omega\text{-cm}$  at 20 V, this performance is certified the field effect. Due to large ionic radius of Pr (0.99 Å) as compared to  $\text{Fe}^{3+}$  (0.645 Å), it has been described that Pr ions occupy octahedral sites [29].

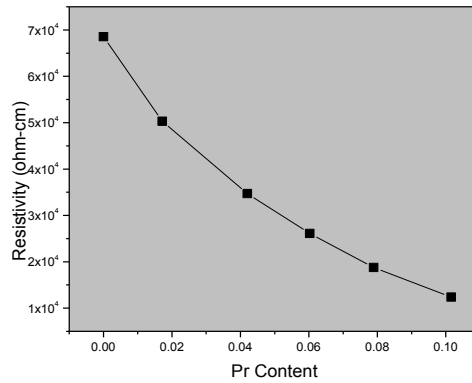
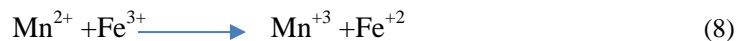


Fig. 5. Resistivity of  $(Sr_{0.5-x}Pr_xBa_{0.5}Fe_{12-y}Mn_yO_{19})$  where  $(x=0.00-0.1, y=0.0-1.0)$ .

The concentration of  $Fe^{3+}$  ions slowly decreases at B-sites when Pr is replaced in place of iron. The hopping rate of shifting of electron will decrease with the decrease of  $Fe^{3+}$  ions concentration. As a result, it increases the dc resistivity with the increase of Pr concentration. The  $Fe^{2+}$  ions' concentration is a typical property of a given material and it depends upon the numerous factors namely amount of substituent, sintering temperature, atmosphere, time and grain size etc. [30]. Another cause for increase in resistivity on mounting Pr is since the activity of Pr ions at B-sites will increase the partition between  $Fe^{3+}$  and  $Fe^{2+}$  ions in fraction to its ionic radius which is dependable with the variation of lattice constant vs. Pr-content. Since the hopping of electrons between ferrous and ferric ions is limited hence both resistivity and activation energy increases. These results are dependable with the results reported by different authors [31, 32]. The probable conduction mechanism in the current samples may be due to hopping of electrons from  $Fe^{2+}$  to  $Fe^{3+}$  and hole shifted from  $Mn^{3+}$  to  $Mn^{2+}$  ions [33, 34].



Combining the exceeding two equations,



The possible reason for the decrease in resistivity in these ferrites may be due to the existence of  $Fe^{2+}$  ions created during sintering producer.

### 3.2.3. Activation Energy

The activation energies were calculated from the slope of the Arrhenius plots voltages (5V) shown in Fig. 6. It is creating that the activation energy and the electrical resistivity vs. Pr concentration explain similar performance. It is clearly observed that the sample contains with higher resistivity has higher values of activation energies and vice versa [35]. Hence the substitution of Pr ions, the higher values of activation energies at higher Europium concentration explain the strong blocking of the conduction method between ferrous and ferric ions. A logical result for the rising behavior of activation energy can be attributed to the increase in lattice constant. It has been described that in ferrites, the whole ionic distance increases during increase in the values of lattice constant [36].

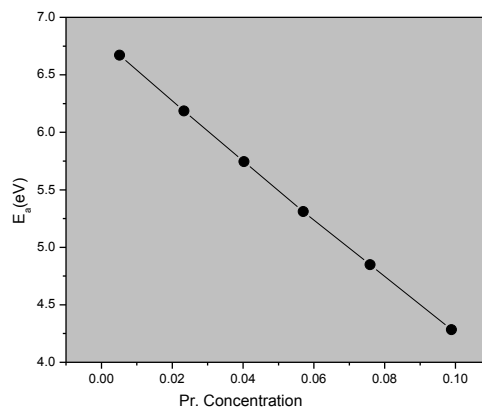


Fig. 6. Activation energy of  $(Sr_{0.5-x}Pr_xBa_{0.5}Fe_{12-y}Mn_yO_{19})$  where  $(x=0.00-0.1, y=0.0-1.0)$ .

#### 4.2. DC Conductivity

Usually, the electrical properties of the ferrite materials depend upon chemical composition, and preparation, technique sintering temperature, and grain size, etc. Fig. 7 reveals that by increasing temperature, the conductivity of ferrite increases, it shows that these ferrites have properties like semiconductors [37, 38].

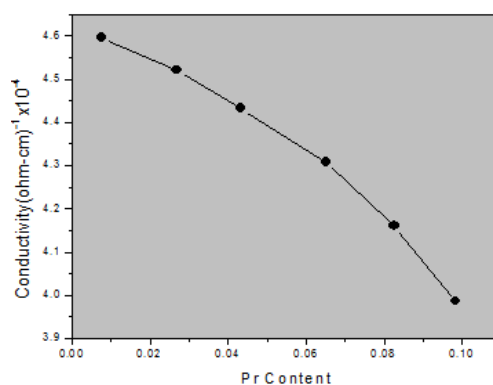


Fig. 7. Variation of DC conductivity  $(Sr_{0.5-x}Pr_xBa_{0.5}Fe_{12-y}Mn_yO_{19})$  where  $X=0.00-0.1, Y=0.0-1.0$ .

At room temperature the conductivity of ferrite is due to impurities, whereas at high temperature conductivity is due to polaron hopping. The conductivity in ferrites can be described by Verwey's hopping mechanism [39]. Verwey, theory explain that conductivity of electron in ferrite is mainly due to hopping of electrons between ions of the same element present in supplementary than one valence state, distributed by chance over crystallographic different lattice sites. The M-type ferrite describes crystallizes in a hexagonal structure with 64 ions per unit cell on 11 different symmetry sites. The 24  $Fe^{3+}$  atoms are spread over five dissimilar sites: three octahedral (B) sites (12k, 2a and 4f2), one tetrahedral (A) site (4f1) and one new type of interstitial (C) site (2b) which is not establish with spinel and is enclosed by five oxygen ions constituting a trigonal bipyramid. In the hexagonal structure two tetrahedral sites are bordering to each other and for these two only one metal ion is existing. This metal ion now presents halfway between them, amidst the three oxygen ions. The distance between two metal ions at (B) site is lesser than the distance between a metal ion at (B) site and another metal ion at (A) site. The electron hopping between (A) and (B) sites below natural conditions therefore has a less possibility compared with that for (B)–(B) hopping. Hopping between (A)–(A) sites does not present for the simple reason that there are only  $Fe^{3+}$  ions at (A) site and any  $Fe^{2+}$  ions produced during processing preferentially engage (B) sites only. The hopping chance depends upon the partition between ions involved and

the activation energy [40]. So, at high temperature, the hopping between  $\text{Fe}^{2+} \leftrightarrow \text{Fe}^{3+}$  and  $\text{Pr}^{2+} \leftrightarrow \text{Pr}^{3+}$  is also possible.

## 5. Dielectric properties

### 5.1 Dielectric constant

Fig. 8 shows the dielectric constant versus frequency for  $(\text{Sr}_{0.5-x}\text{Pr}_x\text{Ba}_{0.5}\text{Fe}_{12-y}\text{Mn}_y\text{O}_{19})$ , ( $x = 0.00-0.10$ ;  $y = 0.00-1.00$ ) at room temperature  $27^\circ \text{C}$ . The dielectric constant decreases through increasing frequency. At the stage of high frequencies, the dielectric constant seems to be independent of frequency. This presentation of the samples is performance to the Maxwell–Wagner model [41]. According to the Maxwell–Wagner model the dielectric materials contains with heterogeneous structure and it can be thought that good conducting grains separated by highly resistive thin grain boundaries. In this technique, the applied voltage on the sample drops mostly across the grain boundaries and a space charge polarization is reputable at the grain boundaries. The space charge polarization is made by the free obtainable charges on the grain boundary and the conductivity of the sample. This is due to main fact that in ferrites, because space charge polarization directly depends upon  $\text{Fe}^{2+}$  ions concentration in a grain. It is, however, experimentally observed that  $\text{Pr}^{2+}$  ions have strong preference to live in tetrahedral A-sites therefore, concentration of  $\text{Fe}^{2+}$  ions on tetrahedral site decreases. Therefore, electric polarization decreases hence the dielectric constant also decreased. This might also be due to the source that  $\text{Mn}^{3+}$  ions did not contribute in the conduction process because impedes is the motion of charge carriers [42, 43]. Koops [44] explained that the result of grain boundaries is predominant at lower frequencies, due to higher dielectric constant for thinner grain boundaries. Higher dielectric constants decrease due to the penetration depth of the electromagnetic waves by increasing the skin effect. Therefore, the much lower dielectric constants obtained for the ferrites deserve their application at of  $\text{Fe}^{2+}$  ions on tetrahedral site decreases. Consequently, due to decrease in electric polarization, the dielectric constant also decreased. This is main reason due to the  $\text{Mn}^{3+}$  ions did not participate in the conduction process hence impedes the motion of charge carrier higher frequencies.

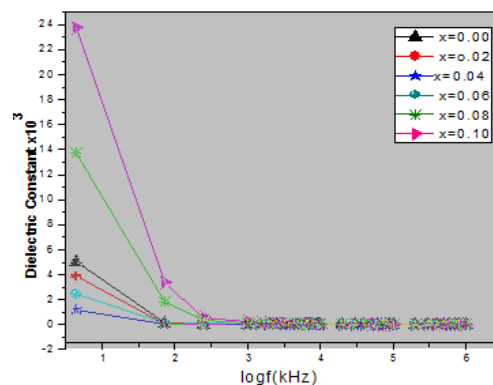


Fig. 8. Dielectric constant versus frequency of  $\text{Sr}_{0.5-x}\text{Pr}_x\text{Ba}_{0.5}\text{Fe}_{12-y}\text{Mn}_y\text{O}_{19}$  where ( $x=0.00-0.1$   $y=0.0-1.0$ ) ferrites.

### 5.2. Dielectric Loss

Fig. 9 shows Dielectric loss versus frequency for  $\text{Sr}_{0.5-x}\text{Pr}_x\text{Ba}_{0.5}\text{Fe}_{12-y}\text{Mn}_y\text{O}_{19}$  where ( $x=0.00-0.1$   $y=0.0-1.0$ ) ferrites. Dielectric loss is very important part of the total core loss in magnetic materials. Because, of low core losses, low dielectric losses are admirable. The dielectric loss decreased substantially when increasing frequency and still reached constant value [45]. Dielectric loss is showing the energy dissipation in the dielectric system. For all the samples, is decreased consequently with increasing frequency. This reason is clarifying that decrease in  $\text{Fe}^{2+}$  ions concentration, due to responsible for conduction losses, because of the increase in  $\text{Mn}^{3+}$  and

$\text{Pr}^{+2}$  contents as explained earlier [46]. That the low-frequency region resultant to high resistivity due to grain boundaries, extra energy is necessary for electron exchange between  $\text{Fe}^{3+}$  and  $\text{Fe}^{2+}$  ions, consequently that the energy loss is high. Due to the high frequency range, corresponding at low resistivity and less energy is required for electron transfer exchange between ferrous and ferric ions in the grains. Hence, the energy loss is minimized. Because of dielectric loss is an important part of the total core loss in magnetic materials [47]. Hence, for low core loss, low dielectric losses are attractive. The example of dielectric loss is similar to those of the actual part of dielectric constant. The Hopping electrons result is increased in a local displacement into the direction of extent electric fields because an increase in electric polarization and accordingly enhanced the dielectric loss. Hudson [48] has explains that the dielectric losses in ferrite are normally reflected in the conductivity measurements anywhere the highly conductive materials exhibited high losses and vice versa.

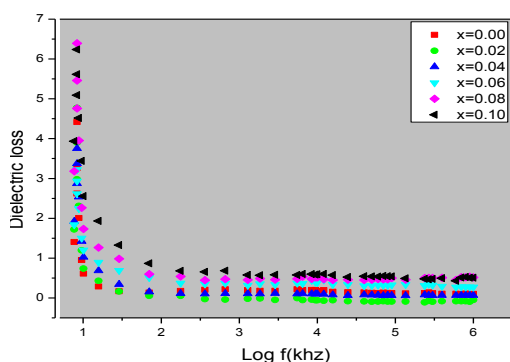


Fig. 9. The Dielectric loss versus frequency of  $(\text{Sr}_{0.5-x}\text{Pr}_x\text{Ba}_{0.5}\text{Fe}_{12-y}\text{Mn}_y\text{O}_{19})$  where  $(x=0.00-0.1, y=0.0-1.0)$  ferrites.

## 6. Conclusions

The samples  $(\text{Sr}_{0.5-x}\text{Pr}_x\text{Ba}_{0.5}\text{Fe}_{12-y}\text{Mn}_y\text{O}_{19})$  where  $(X=0.00-0.1, Y=0.0-1.0)$  ferrites prepared by sol-gel auto combustion method: results in enhanced structural, electrical and dielectric properties.

XRD patterns of samples indicate that the peaks match well with the standard patterns of M-type hexaferrites compared with PDF card No (00-001-0574). The extra peaks appeared in samples having x/y concentrations above 0.6, were also indexed and matched to ICDD PDF#00-002-0692 of  $\text{PrFeO}_3$ .

Lattice parameter lies in the range because  $a = (5.9 - 5.94) \text{ \AA}$  and  $C = (23.28 - 23.32) \text{ \AA}$ . SEM indicates well defined and homogenized shape of the hexa-ferrites. Samples 2 and 3 also shows some hexagonal particles. Resistivity lies in range about the room temperature resistivity enhanced with the increasing of Pr-contents from and  $1 \times 10^{+4}$  to  $7 \times 10^{+4} \Omega\text{-cm}$  at 5 V. Conductivity at room temperature the conductivity of ferrites is due to impurity, as at higher temperature conductivity is occurring through polaron hopping.

Dielectric constant according to Maxwell–Wagner model the dielectric substance contains with heterogeneous structure thought that good conducting grains separated by highly resistant thin grain boundaries. Dielectric losses are very essential part of the sum of the core loss in magnetic materials, as according to Hudson theory.

It appears from the consequences that the dual mixture of (PrMn) ions can trigger the structure, electrical and dielectric properties. Hence the conduction in  $\text{Sr}_{0.5-x}\text{Pr}_x\text{Ba}_{0.5}\text{Mn}_y\text{Fe}_{12-y}\text{O}_{19}$  is gives rise to hopping conduction mechanism of localized charge carriers.

## References

- [1] G. Albnese, A. Dariu, F. Licci, S. Rinaldi, *IEEE Trans. Magn.* **14**, 710 (1978).
- [2] H. J. Kown, J. Y. Shin, J. H. Oh, *J. Appl. Phys.* **75**, 6109 (1994).
- [3] E. Naiden, V. Maltsen, G. Ryabtsen. *Phys. Stat Sol.* **120**, 209 (1990).
- [4] K. Yoon, D. Lee, H. Jung, S. Yoon, *J. Mater Sci.* **27**, 2941 (1992).
- [5] J. Ding, D. Maurice, W. F. Miao, P. G. Mc Cormick, R. J. Street, *Magn. Magn. Mater.* **150**, 417 (1995).
- [6] G. Mendoza Suarez, J. A. Matutes-Aquino, J. I. Escalante-Garcia, H. Mancha-Molinar, D. Rios-Jara, K. K. Johal, *J. Magn. Magn. Mater.* **223**, 55 (2001).
- [7] S. M. Abbas, A. K. Dixit, R. Chatterjee, T. C. Goel, *J. Magn. Magn. Mater.* **309**, 20 (2007).
- [8] J. Kulikowski, *J. Magn. Magn. Mater.* **41**, 56 (1984).
- [9] S. Ruan, B. Xu, H. Suo, F. Wu, S. Xiang, M. Zhao, *J. Magn. Magn. Mater.* **212**, 175 (2000).
- [10] M. A. El Hiti, *J. Magn. Magn. Mater.* **192**, 305 (1996).
- [11] M. J. Iqbal, M. N. Ashiq, I. H. Gul, *J. Magn. Magn. Mater.* **322**(13), 1720 (2010).
- [12] R. Valanzuela, *Magnetic ceramics*. Cambridge University Press, Cambridge (2005).
- [13] M. J. Iqbal, M. N. Ashiq, *Chem. Eng. J.* **136**, 383 (2008).
- [14] M. U. Islam, F. Aen, S. B. Niazi, M. Azhar Khan, M. Ishaque, T. Abbas, M. U. Rana, *Mater. Chem. Phys.* **109**, 482 (2008).
- [15] S. Hussain, A. Maqsood, *J. Magn. Magn. Mater.* **316**, 73 (2007).
- [16] Hasan M. Khan, M. U. Islam, Y. Xu, M. N. Ashiq, I. Ali, M. Asif Iqbal, M. Ishaque, *Ceram. Intl.* **40**, 6487 (2014).
- [17] Hasan M. Khan, M. U. Islam, Y. Xu, M. A. Iqbal, I. Ali, *J. Alloys Compd.* **589**, 258 (2014).
- [18] S. Sindhu, M. R. Anantharaman, B. P. Thampi, K. A. Malini, P. Kurian, *Bull. Mater. Sci.* **25**, 599 (2002).
- [19] G. G. Wang, J. M. Wang, W. Q. Mao, L. Q. Liu, J. Q. Zhang, C. N. Cao, *Acta Phys.* **21**, 1285 (2005).
- [20] C. J. Curtis, J. Wang, D. L. Schutz, *J. of Electrochemical Soc.* **151**, A590 (2004).
- [21] N. Rezlescu, C. Doroftei, E. Rezlescu, P. D. Popa, *Phys. Status Solidi* **15**, 3844 (2006).
- [22] K. Nadeem, L. Ali, I. Gul, S. Rizwan, M. Mumtaz, *J. Non-Cryst. Solids* **404**, 72 (2014).
- [23] G. Mumeu, K. Sertel, J. L. Volakis. A. Figotin, I. Vitebsky, *IEEE Trans. Antennas Propaga.* **2**, 1935 (2004).
- [24] A. B. Gadkari, T. J. Shinde, P. N. Vasmbekar, *Materials Chemistry and Physics* **114**, 505 (2009).
- [25] M. N. Ashiq, M. J. Iqbal, I. H. Gul, *J. Alloys Comp.* **487**, 341 (2009).
- [26] N. Rezlescu, C. Doroftei, E. Rezlescu, P. D. Popa, *Phys. Status Solidi* **15**, 3844 (2006).
- [27] T. R. Wagner, *J. Solid State Chem.* **136**, 120 (1998).
- [28] K. Nadeem, H. Krenn, M. Shahid, I. Letofsky-Papst, *Solid State Sci.* **19**, 27 (2013).
- [29] N. Rezlescu, E. Rezlescu, *Ferrites, Solid State Communications* **88**, 139 (1993).
- [30] U. Ghazanfar, S. A. Siddiqi, G. Abbas, *Materials Science and Engineering B* **118**, 132 (2005).
- [31] N. Rezlescu, E. Rezlescu, P. D. Popa, L. Rezlescu, *Journal of Alloy and Compounds*, 657 (1998).
- [32] N. Rezlescu, E. Rezlescu, C. Pasnicu, M. L. Craus, *Journal of Physics: Condensed Matter* **6**, 5707 (1994), A 672 (1997).
- [33] Hasan M. Khan, M. U. Islam, Yongbing Xu, M. Asif Iqbal, Irshad Ali, Muhammad Ishaque, Muhammad Azhar Khan, *J. Sol-Gel Sci. Technol.* **75**(2), 305.
- [34] D. Ravinder, P. V. B. Reddy, *Materials Letters* **57**, 4344 (2003).
- [35] B. Ramesh, D. Ravinder, *Materials Letters* **62**, 2043 (2008).
- [36] E. Rezlescu, N. Rezlescu, P. D. Popa, L. Rezlescu, C. Pasnicu, *Physica Status Solidi*.
- [37] T. Abbas, M. U. Islam, M. A. Chaudhry, *Mod. Phys. Lett. B* **9**(22), 1419 (1995).
- [38] J. Smit, H. P. J. Wijn, *Ferrites*, Wiley, New York, 1959.
- [39] E. J. W. Verwey, J. H. De Boer, *Rec. Trans. Chem. Des. Pays. Bas.* **55**, 531 (1936).
- [40] A. Lakshman, P. S. V. Subha Rao, B. P. Rao, K. H. Rao, *J. Phys. D. Appl. Phys.* **38**, 673 (2005).
- [41] M. J. Iqbal, S. Farooq, *Mater. Chem. Phys.* **118**, 308 (2009).

- [42] Hasan M. Khan, M. U. Islam, Yongbing Xu, M. Asif Iqbal, Irshad Ali, Muhammad Ishaque, Muhammad Azhar Khan, Nazia Karamat, Imran Sadiq, *J Sol-Gel Sci Technol.* **8**(1) , 151 (2016).
- [43] M. A. Ahmed, E. Ateia, S. I. El-Dek, *Mater. Lett.* **57**, 4256 (2003).
- [44] M. K. Shobana, S. Sankara, V. Rajendran, *Mater. Chem. Phys.* **113**, 1041 (2009).
- [45] V. R. K. Murthy, J. Shobanadri, *Phys. Status Solid A* **36**(2), 133 (1976).
- [46] K. W. Wagner, *Ann. Phys.* **40**, 817 (1913).
- [47] A. A. Sattar, A. H. Wafik, H. M. El-Sayed, *J. Mater. Sci.* **36**, 4703 (2001).
- [48] A. S. Hudson, *Marconi Rev.* **37**, 43 (1968).